tvst

Article

A Depth-Dependent Integrated VF Simulation for Analysis and Visualization of Glaucomatous VF Defects

Ping Liu[1], Allison McKendrick[1], Anna Ma-Wyatt[3], and Andrew Turpin[2]

[1] Department of Optometry and Vision Sciences, The University of Melbourne, Victoria, Australia
[2] School of Computing and Information Systems, The University of Melbourne, Victoria, Australia
[3] Department of Psychology, The University of Adelaide, South Australia, Australia

Correspondence: Andrew Turpin, Department of Computing and Information Systems, The University of Melbourne, Victoria, Australia.
e-mail: aturpin@unimelb.edu.au

Received: February 4, 2019
Accepted: November 24, 2019
Published: February 12, 2020

Keywords: functional visual field; volume perimetry; simulation; glaucoma

Citation: Liu P, McKendrick A, Ma-Wyatt A, Turpin A. A depth-dependent integrated VF simulation for analysis and visualization of glaucomatous VF defects. Trans Vis Sci Tech. 2020;9(3):8, https://doi.org/10.1167/tvst.9.3.8

Purpose: Visual fields (VF) are measured monocularly at a single depth, yet real-life activities require people to interact with objects binocularly at multiple depths. To better characterize visual functioning in clinical vision conditions such as glaucoma, analyzing visual impairment in a depth-dependent fashion is required. We developed a depth-dependent integrated VF (DD-IVF) simulation and demonstrated its usefulness by evaluating DD-IVF defects associated with 12 glaucomatous archetypes of 24-2 VF.

Methods: The 12 archetypes included typical variants of superior and inferior nasal steps, arcuate and altitudinal defects, temporal wedge, biarcuate, and intact VFs. DD-IVF simulation maps the monocular 24-2 VF archetypes to binocular ones as a function of depth by incorporating three parameters of fixation, object, and interpupillary distances. At each location and depth plane, sensitivities are linearly interpolated from corresponding locations in monocular VF and returned as the higher value of the two.

Results: The simulation produced 144 DD-IVFs for multiple depths from combinations of 12 glaucomatous archetypes. The DD-IVFs are included as a Shiny app in the binovisualfields package. The number of impaired locations in the DD-IVFs varied according to the overlap of VF loss between eyes.

Conclusions: Our DD-IVF program revealed binocular functional visual defects associated with glaucomatous archetypes of the 24-2 pattern and is designed to do the same for empirically measured VFs. The comparison of identified visual impairments across depths may be informative for future empirical exploration of functional visual impairments in depth in glaucoma and other conditions leading to bilateral VF loss.

Translational Relevance: Our DD-IVF program can reveal depth-dependent functional visual defects for clinical vision conditions where 24-2 test patterns are available.

Introduction

Although monocular visual field (VF) testing is critical for the diagnosis and monitoring of change of a range of ophthalmic and visual pathway diseases, such as glaucoma, the binocular VF (BVF) is more closely related to patients' subjective visual experiences, visual functioning, and disability in daily life.[1] This is not surprising, given that VF defects in one eye are frequently compensated for by corresponding locations with normal sensitivity in the other.[2] Being diagnosed and regularly assessed for sight-threatening disorders can cause distress in some patients given the irreversible nature of many ophthalmic conditions.[3] Hence, providing a realistic perspective of a patient's visual performance through accurate quantification of functional VF defects is important for patient care, as is developing compensatory strategies and rehabilitation protocols to help minimize the impact of visual impairments on quality of life.

Although it is possible to measure VFs binocularly (e.g., see Esterman[4]), resource constraints typically limit such testing to situations where there is a need to evaluate VF status for fitness to drive, or other occupational task reasons. When not measured directly, estimated integrated VFs (IVF) composed from measured monocular VFs in each eye have been

used to estimate patients' BVFs.[4–6] These methods have been shown to provide a reasonable estimation of BVF status.[7] Nevertheless, neither clinically measured BVFs nor estimations of IVF provide information regarding binocular sensitivity for depths that deviate from the fixation plane. It has been shown that an intact BVF at the plane of fixation (or the perimeter surface) does not exclude the presence of BVF defects on a different depth plane.[8] Conversely, the presence of an impaired BVF location at the fixation plane does not mandate impaired vision at the same location for every other depth plane.[9] It is, therefore, possible that objects appearing at impaired locations on distance planes different from the current fixation plane are at risk of being undetected by patients, which could lead to reduced efficiency in daily functioning and even accidents.

Volume scotomas are regions of three-dimensional space that are of reduced or no visibility to the observer because images of objects in such regions either fall onto areas with impaired sensitivity in the retinas or into a blind area with no binocular overlap. Mapping of volume scotomas in the linear three-dimensional space is referred to as volume perimetry.[10] The magnitude and location of the volume scotomas varies with the instantaneous fixation distance or the convergence of eyes. It has been argued that since the volume VF (VVF) takes into account depth in space, it yields the closest approximation of a person's real field of view.[10]

Complete VVF testing, however, is impractical in standard clinical practice. There is no report on performing a complete volume perimetry for distances ranging from very close (e.g., 14 cm) to very far (e.g., 1000 cm and beyond). Direct measurement of VVF at representative planes has only been reported in one recent article.[9] Three slices of VF at the plane of fixation, a plane anterior to fixation, and a plane posterior to fixation were measured in three patients with a complicated set up.[9] The study found that anterior and posterior VVFs could vary substantially from conventional binocular perimetry measured at the fixation plane, revealing impaired areas not otherwise identified. The study, however, did not recruit typical glaucoma patients, and consequently cannot shed light on typical VVF defects likely to be experienced by people with glaucoma, the most common cause of VF loss.[11]

VF deficits in depth can be estimated from monocular VF measurements. One previous study outlined the methods for constructing IVF by superimposing two monocular field maps with successive transverse sectional views and referred to these maps as retinocentric binocular field maps.[10] Although theoretical computation of depth-dependent IVF (DD-IVF) from two monocular VF results is possible, to the best of our knowledge, there is no existing simulation program available in the public domain that reads standard clinically measured monocular VFs and estimates how these two disparate, inhomogeneous VFs can be combined to produce a single IVF as a function of depth.

We have developed a new method of simulating DD-IVFs by mapping measured monocular VFs of the 24-2 pattern to binocular ones as a function of depth using established principles of binocular geometry. This simulation incorporates the three important parameters: fixation distance, object distance, and interpupillary distance (IPD) to estimate BVF defects at various depths that may otherwise be left unidentified. The model not only simulates BVF for any specified fixation distance plane, but also estimates BVF on any object distance plane other than the fixation plane. In this model, a simplified case is adopted where foveal fixation is present in both eyes and the eyes converge symmetrically at the horizontal center of the fixation plane. Although IPD is helpful for more precise simulation of DD-IVFs, it can be estimated from average population values for both genders if not available for a given patient.

Three typical distance ranges were chosen for the anterior, fixation, and posterior planes in our visualization application. The fixation distance was set within the range of 41 to 76 cm because tasks of daily living important for manipulating actions and social interactions predominantly use fixation distances within this range compared with far distances within visual scenes.[12–17] Correspondingly, the anterior and posterior plane distance ranges were set as between 14 (i.e., very close) to 40 cm and 71 to 150 cm, respectively. To provide a ready reference for clinicians, we have applied the simulator to pairs of eyes with 12 patterns of typical glaucomatous damage as measured on the 24-2 test pattern, deriving DD-IVFs for an anterior (25 cm), a fixation (60 cm), and a posterior (100 cm) plane.

Methods

Binocular Field Simulation

For simplicity, IVFs are only simulated in the scenario where the eyes converge symmetrically at the center of the horizontal horopter with the head in a straight-ahead and upright position. Our simulation does not calculate possible field positions of occlusions that may occur when the eyes converge to close range distance. In all cases illustrated herein, f represents the distance from the plane of the eyes to the point of

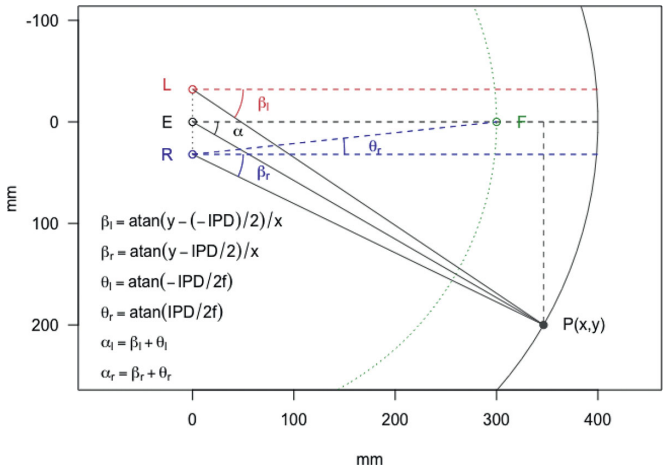

Figure 1. Monocular horizontal coordinates calculation. The schematic representation depicts the top-down view of the left, right and IVFs with L, R, and E denoting the origin of corresponding VF. The vertical dotted line represents the x axis with the middle of the interpupillary distance (E) as its origin and the top indicating left (negative) and bottom right (positive) respectively. For any given location P with horizontal coordinate α on any distance plane in the IVF, the corresponding horizontal coordinate in the left and right monocular VF (α_l and α_r respectively) is defined as the sum of the angle that location P forms with respective eye viewing axis when fixating at infinity (β_l and β_r) and the convergence angle for respective eye (θ_l and θ_r) for a given fixation distance (from E to the center of the fixation plane F).

fixation (E to F in Fig. 1) and *dp* represents the distance from the eye plane to an object plane in millimeters (E to P in Fig. 1). The origin of the coordinate system for the DD-IVF is set between the two eyes at the middle of the IPD (E in Fig. 1). In all DD-IVFs, the left of the horizontal axis is defined as negative (up in Fig. 1) and right positive.

For some point P(x, y) in the DD-IVF, we have

$$x = dp * cos\left(\frac{\alpha}{180} * \pi\right)$$

$$y = dp * sin\left(\frac{\alpha}{180} * \pi\right)$$

where α is the angle P subtends from E in degrees (30° in Fig. 1).

To find the corresponding points in the left and right VFs, we add the left and right convergence angles, calculated according to

$$\theta_l = tan^{-1}\left(\frac{-IPD}{2f}\right)$$

$$\theta_r = tan^{-1}\left(\frac{IPD}{2f}\right),$$

respectively, to the angles of P from horizontal lines extending from each eye to get

$$\alpha_l = tan^{-1}\left(\left(y + \frac{IPD}{2}\right)/x\right) + \theta_l$$

$$\alpha_r = tan^{-1}\left(\left(y - \frac{IPD}{2}\right)/x\right) + \theta_r.$$

Figure 1 illustrates these equations.

The dB value(s) of location P are linearly interpolated from respective monocular VF at the respective horizontal coordinate α_l and α_r. The interpolation is across space (over the hill of vision) which we assume to be approximately linear on the dB scale for the small distances (maximum distance of 6°) we are dealing with. Take the location (3, 3) in the anterior IVF in Figure 3, for example, with the fixation distance at 600 mm and assuming the IPD to be 62 mm (the population mean for females). The corresponding coordinates of this location in Figure 1 is ($x = 249.6$, $y = 13.1$). The horizontal coordinates of this location in the corresponding left and right monocular VF α_l and α_r are thus 7° and –1°, respectively. For the left VF, the dB values at horizontal locations 3° and 9° are both 0; therefore, the linearly interpolated dB value at 7° is 0 dB too. For the right VF, the dB values at horizontal locations –3° and 3° are 0 dB and 30 dB, respectively. The resulting linearly interpolated sensitivity value at –1° is 10 dB because –1° is four steps away from 3° where the sensitivity is 30 dB.

The final sensitivity value (in decibels) at any simulated integrated location P is determined by the following four rules. In cases where the sensitivity values interpolated from both the left and right VF are available, the sensitivity of location P takes the greater value of the two. If the sensitivity calculated from either left or right VF is missing, but the other is available and is greater than 25 dB, the final sensitivity value is equal to the available value. If, however, this available value is less than 25 dB, the sensitivity at location P is defined as around missing, because it is unknown whether there is, or is not, normal sensitivity in the unmeasured location. If the sensitivity values cannot be interpolated from either monocular VF, the final simulated sensitivity at location P is defined as missing. We define a cut-off of 25 dB as the lower limit of normal threshold.[18]

The DD-IVFs are calculated at locations with horizontal coordinates of –57° to 57° with a step size of 6° and vertical coordinates the same as in the commonly used 24-2 test pattern.

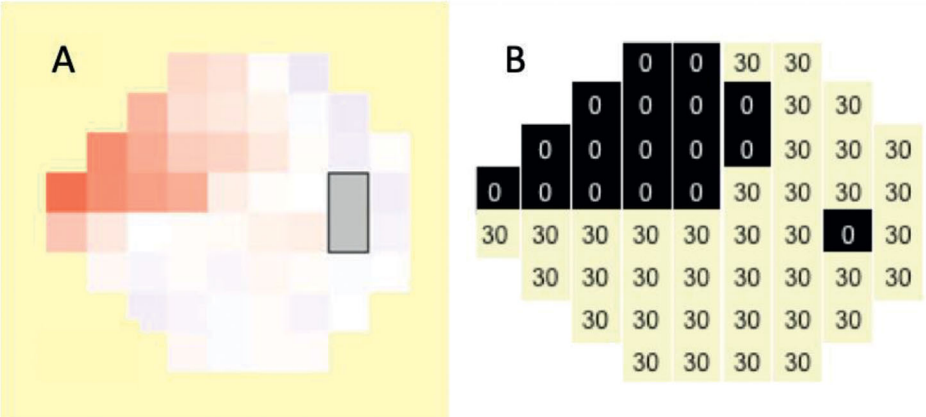

Figure 2. Archetype 3 from Figure 6 of Elze et al.[19] and its recoded binary version included in the current simulation.

Glaucomatous Archetypes

Using this technique, DD-IVFs were simulated using 12 out of the 17 archetypes identified in a previous study.[19] Archetypes 7, 11, 12, 15, and 17 identified in their article were excluded for various reasons. Archetype 7 was excluded because of its similarity to archetype 13. For simplicity, only archetype 13 was included here. Archetype 11 resembles an artefact from lens–rim or eyelid occlusion, and therefore is excluded. Archetypes 12 and 15 are excluded because they are more typical of cortical lesions than glaucomatous VF defects. The resulting 12 archetypes are ordered by VF defect location from superior to inferior and nasal to temporal as shown in Figures A1, A2, and A3.

To simplify the DD-IVF simulation with the 12 archetypes, we chose to recode the archetypes using a binary instead of the original gradient coding system for visual sensitivity values. Impaired VF locations were assigned 0 dB and relatively healthy VF locations 30 dB. This dichotomizing judgment was applied to all 12 archetypes based on both expert knowledge of glaucoma vision loss and the color-coding values in Figure 6 of the study.[19] The coordinates of the center of blind spot were assumed at 15° temporal and 3° below the horizontal meridian. Although a blind spot is not a glaucomatous defect, it leads to functional IVF defects when interacting with glaucomatous defects in the other eye. It is therefore coded as 0 dB in our binary archetypes. An example of the original archetype (archetype 3) from the study[19] and its dichotomized counterpart (archetype 2 in the current study) is shown in Figure 2. Although we used these archetypes (with only six possible dB values 0, 5, 10, 15, 20, and 25 for any location in the resulting IVFs) to illustrate the usefulness of the simulator, our simulator is designed to take pairs of empirically measured VFs as input. Correspondingly, we have adopted a gradient color-coding scheme similar to that used elsewhere to describe VF defects,[20] allowing precise representation of sensitivity variations.

Results

The simulated DD-IVFs with the 12 archetypes, are provided in a Shiny app included in the binovisualfields R package available at (https://people.eng.unimelb.edu.au/aturpin/opi/index.html).[21] The shiny app is also available online at (https://people.eng.unimelb.edu.au/aturpin/opi/binovisualfields.html). Here we present the simulated DD-IVFs for the 12 × 12 archetype interactions at an anterior object distance plane of 25 cm, a fixation plane of 60 cm, and a posterior object distance plane at 100 cm.

The simulation and visualization revealed some important functional VF defect patterns with the included glaucomatous VF archetypes. The pictorial summaries of the 144 IVFs for the three planes are presented in Figures A1, A2 and A3 with the 12 archetypes ordered by VF defect location from superior to inferior and nasal to temporal. The simulated IVF patterns are symmetric with respect to the main diagonal. As expected, when visual defects of the two eyes do not share vertical coordinates, there are virtually no resulting visual defects in the DD-IVFs, except for possible interactions between the blind spot in the eye with superior VF defect and the inferior VF defect in the other. Impaired locations are predominantly found in archetypes both with superior nasal defects or inferior nasal defects. When one eye displaying an archetype with minor visual defect limited to the temporal area (archetypes 11

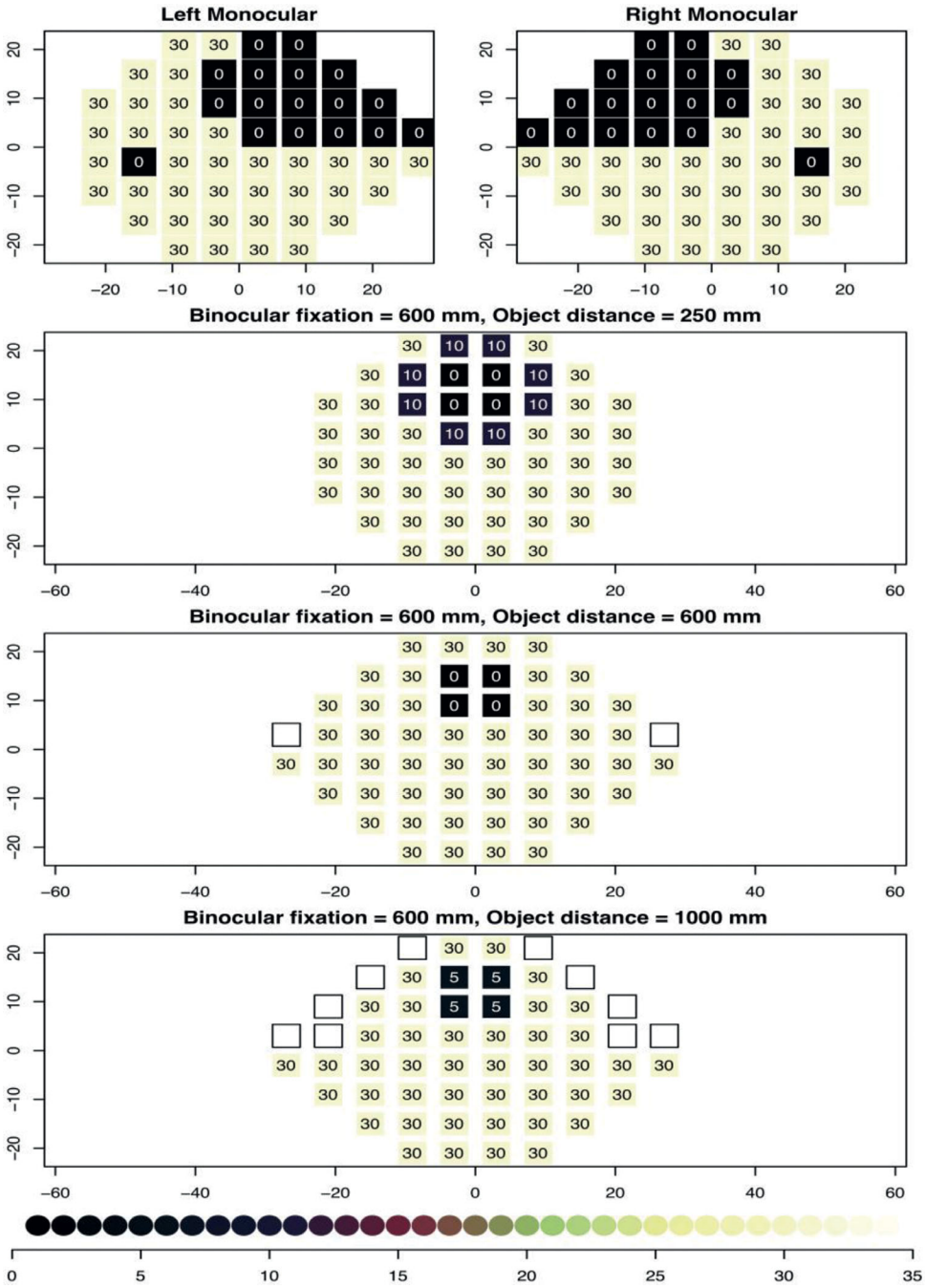

Figure 3. IVFs for the anterior, fixation and posterior planes for archetype 2 (superior nasal defect). Locations in the DD-IVF subplots are color coded with darker values representing lower dB values, that is, *black*, 0 dB; *green*, 20 dB; and *yellow*, 30 dB. Any location with a missing dB value is denoted by a hollow square.

or 12) and the other presenting nasal visual defect (archetypes 6, 7, 8, 9, and 10), the IVF visual defect is generally limited to the area corresponding to the temporal defect.

Across the three planes, IVF patterns on the anterior plane differ more from those on the fixation plane than the posterior plane. For bilateral nasal defects (archetypes 2–10), while the IVFs display minor visual defects near the vertical meridian on the fixation and far plane, such defects are generally more widespread on the anterior plane at 25 cm (see Fig. 3 for IVF pattern variations across the anterior, fixation and posterior planes for archetype 2 for an example). Similarly, for interactions between archetypes of superior VF defect in one eye and inferior ones in the other, the DD-IVF defect around the blind spot area becomes more widespread on the anterior plane compared with the fixation plane.

The number of impaired locations (the *black squares*) at the three representative planes and the number of locations with missing values (the *hollow squares*) are summarized in Appendix A.

Discussion

The estimation of BVF from monocular VF data as a function of depth was proposed decades ago,[10] but is rarely considered despite the likely importance of VF deficits in depth for tasks of daily living. A readily accessible method for the simulation and visualization of central DD-IVFs is described in this article and included in the binovisualfields package. Our simulator enables the estimation of DD-IVFs from any empirically measured pairs of 24-2 test pattern. The open source R Package (The R Foundation, Vienna, Austria) is freely available for all researchers and clinicians. The usefulness of the simulator is demonstrated via the exploration of VF defects at different depth planes that would be present in typical glaucomatous eyes. The simulation code is provided as an example in the Appendix B. Researchers and clinicians can easily modify the example code to visualize real patient data for their research or healthcare purposes.

Although glaucomatous VF archetypes with dichotomized dB values were used to simulate DD-IVFs in the current study, the simulator is designed to be used with empirical data for clinical and research purposes for any 24-2 VF data. With empirical data, this simulator will provide more fine-grained estimation for depth-dependent functional VF defects. For clinical consultation, patients with binasal superior (e.g., archetypes 2 and 3) or inferior (archetype 9) visual defects may experience a central visual defect to different degrees on the anterior plane than fixation plane depending on individual patient's interpupillary distance and chosen fixation distance. When such individual data are available, our simulator can provide customized estimation of functional VF defect to guide clinical consultation and develop potential compensatory strategies. For research purposes, one interesting application may be to evaluate how well DD-IVF defects correlate with the quality of life and potentially with typical laboratory measurements of tasks of daily living, for example, sandwich making.[22]

It is worth noting that the current simulation assumes a simplified scenario where foveal fixation exists in both eyes and the eyes converge symmetrically at the center of the fixation plane. Consequently, the simulation may be more readily applicable to neural ocular diseases where foveal fixation is usually present, for example, glaucoma, than others such as central field loss, as occurs in age-related macular degeneration, particularly when the two monocular preferred retinal loci may not be in corresponding retinal areas.[23,24] In case of glaucomatous VF with defects in the macular region, which are likely to be captured on 10-2 but not on 24-2 test pattern, our simulation can computationally be adapted for 10-2 pattern data. Considering that defects are so close to the fovea, empirical testing, however, is essential for evaluating the applicability of our model to such scenarios. Depth-dependent visual sensitivity variation in central vision important for fine visual or occupational tasks may need more fine-tuned simulation incorporating more variables such as ocular dominance and binocular summation and a much finer spatial scale to reasonably reflect performance in central visual tasks in real life.

Our DD-IVF simulation using the 12 glaucomatous archetypes revealed various patterns of DD-IVF defects depending on the archetype. The number of locations with impaired vision as well as the number of locations with missing values varies depending on the archetype interaction and objection distance. As Figure A7 shows, certain archetype interactions display more DD-IVF defects on the anterior plane than on the fixation plane. For example, IVF for bilateral superior nasal step (archetype 2) displays eight more impaired locations on the anterior plane than on the fixation plane. Similarly, bilateral inferior nasal step (archetype 9) produces six more impaired locations on the anterior plane than on the fixation plane although the number of impaired locations in archetype 9 is relatively moderate. Given that such VF defects are more prominent on the anterior plane, they are more likely to affect patients when constant changing of fixation for close range manipulation and interaction is required, for example, near work with small hand tools. Similarly, as the object plane moves away from the fixation plane, the area of the binocular overlap decreases. This results in more locations with missing values on the anterior plane and posterior plane than on the fixation plane as shown in Figures A8, A9 and A10 respectively. When evaluating the DD-IVF defects across object distance planes, the number of locations with impaired vision and the number of locations with missing values need to be considered jointly to assess functional VF defects revealed by the simulation.

We used the glaucomatous archetypes to produce an overview of the types of defects that might arise bilaterally in glaucoma. The archetypes present common patterns of glaucomatous VF defects and the associated DD-IVF defects revealed by our program

have provided a reasonable approximation of the DD-IVF defects likely to be experienced by patients with glaucoma. These are not the only defects that might arise and might not represent any given individual patient. Hence, the open access availability for researchers/clinicians to input their own empirical VFs and visualize the outcomes for any given patient.

The current DD-IVF simulation demonstrates certain advantages over existing IVF simulations. All existing IVF simulations are only performed on one fixation plane, and thus cannot shed light on visual sensitivity when fixation distance changes or for scenarios where objects are out of current focus.[7] The impact of fixation change and object distance change on glaucomatous archetype interactions is clearly demonstrated in the interactive Shiny app included in the binovisualfields package. The variations in the DD-IVF defects across the anterior, fixation and posterior planes summarized in Figures A1, A2 and A3 also provide a representative scenario where the DD-IVF defect patterns vary across distance planes depending on glaucomatous archetypes.

The most noticeable advantage of our DD-IVF over real VVF measurements lies in its ease in estimating BVF defects on planes other than the fixation. Complicated procedures impractical for clinical practice are needed to perform real VVF testing as demonstrated previously.[9] In contrast, our simulation can estimate BVF on any object distance plane given any chosen fixation plane using real patient's data instantaneously.

It is important to note that the areas of VF denoted as around normal in our DD-IVF may not necessarily have normal stereopsis or binocular visual function. We classify sensitivity as normal where there is relatively normal differential luminance sensitivity in at least one eye. Indeed, deficits of stereopsis are likely to be far more extensive than the DD-IVF defects illustrated here, because impaired vision in one eye impacts on stereopsis judgments. For example, for the VF scenario shown in Figure 2, the entire superior VF is predicted to have impaired stereopsis, whereas the DD-IVF defect on the anterior plane is significantly reduced in the superior central area. Binocular disparity thresholds measured in a laboratory setting are most sensitive in a range that is within peripersonal space; hence, deficits in stereopsis may impact daily function, even in areas where sensitivity is normal in one eye. In a real–world setting, McKee and Taylor[25] demonstrated that binocular viewing significantly improved depth judgments compared with monocular viewing. There is also evidence that binocular viewing is useful for reaching and pointing in peripersonal space,[26] that is, approximately the fixation range adopted in our simulator. For example, grasping performance in patients with age-related macular degeneration has also been correlated with the amount of stereopsis they retain.[27] Further experimental work is required to determine (1) the impact of DD-IVF defect on stereopsis perception and (2) the impact of the impaired stereopsis in patchy regions of visual fields on daily function and whether compensatory strategies are adopted.

The current study represents a step forward from the existing IVF simulations, but still one of the early steps in the effort of evaluating functional visual defect in neural ocular diseases, such as glaucoma. Future simulation can seek to add parameters to account for factors such as eye dominance and binocular summation to improve the estimation of visual sensitivity values. Such advanced simulation may also be implemented in virtual reality technology to provide a more user-friendly evaluation of functional visual defect for patients.

Acknowledgments

Disclosure: **P. Liu,** None; **A. McKendrick,** Haag-Streit AG (F), Heidelberg Engineering GmBH (F), Centervue SpA (F); **A. Ma-Wyatt,** None; **A. Turpin,** Haag-Streit AG (F), Heidelberg Engineering GmBH (F), Centervue SpA (F)

References

1. Goldberg I, Clement CI, Chiang TH, et al. Assessing quality of life in patients with glaucoma using the glaucoma quality of life-15 (gql-15) questionnaire. *J Glaucoma*. 2009;18:6–12.
2. Sponsel WE, Groth SL, Satsangi N, et al. Refined data analysis provides clinical evidence for central nervous system control of chronic glaucomatous neurodegeneration. *Transl Vis Sci Technol*. 2014;3:1.
3. Glen FC, Baker H, Crabb DP. A qualitative investigation into patients' views on visual field testing for glaucoma monitoring. *BMJ Open*. 2014;4:e003996.
4. Esterman B. Functional scoring of the binocular field. *Ophthalmology*. 1982;89: 1226–1234.
5. Crabb DP, Viswanathan AC, McNaught AI, et al. Simulating binocular visual field status in glaucoma. *Br J Ophthalmol*. 1998;82:1236–1241.
6. Wood JM, Collins MJ, Carkeet A. Regional variations in binocular summation across the visual field. *Ophthalmic Physiol Opt*. 1992;12:46–51.

7. Nelson-Quigg JM, Cello K, Johnson CA. Predicting binocular visual field sensitivity from monocular visual field results. *Invest Ophthalmol Vis Sci*. 2000;41:2212–2221.
8. Arditi A. The adaptive significance of the location of the optic disk. *Perception*. 1987;16:649–654.
9. Satgunam P, Apfelbaum HL, Peli E. Volume perimetry: measurement in depth of visual field loss. *Optom Vis Sci*. 2012;89:e1265–e1275.
10. Arditi A. The volume visual field: a basis for functional perimetry. *Clin Vis Sci*. 1988;3:173–183.
11. Ramrattan RS, Wolfs RCW, Panda-Jonas S, et al. Prevalence and causes of visual field loss in the elderly and associations with Impairment in daily functioning: the Rotterdam Study. *JAMA Ophthalmol*. 2001;11:1788–1794.
12. Wexler M, Ouarti N. Depth affects where we look. *Curr Biol*. 2008;18:1872–1876.
13. Jansen L, Onat S, König P. Influence of disparity on fixation and saccades in free viewing of natural scenes. *J Vision*. 2009;9:29.
14. Sprague WW, Cooper EA, Tosic I, et al. Stereopsis is adaptive for the natural environment. *Sci Adv*. 2015;1:e1400254–e1400254.
15. Howard IP, Rogers BJ. Binocular correspondence and the horopter. In: *Seeing in Depth*. Oxford, UK: Oxford Scholarship Online; 2008.
16. Land MF, Hayhoe M. In what ways do eye movements contribute to everyday activities? *Vision Res*. 2001;41:3559–3565.
17. Hollands MA, Patla AE, Vickers JN. "Look where you're going!" Gaze behaviour associated with maintaining and changing the direction of locomotion. *Exp Brain Res*. 2002;143:221–230.
18. Pricking S. *Age-corrected normal differential luminance values for the entire 80° visual field applying three threshold estimating strategies, using the octopus 900 perimeter [doctoral dissertation]*. Tubingen, Germany: University of Tübingen; 2010.
19. Elze T, Pasquale LR, Shen LQ, et al. Patterns of functional vision loss in glaucoma determined with archetypal analysis. *J Royal Soc Interface*. 2015;12.
20. Racette L, Fischer M, Bebie H, Holló G, Johnson C, Matsumoto C. *Visual Field Digest*. 6th ed. Köniz, Switzerland: Haag-Streit. 2016:105.
21. Turpin A, Artes PH, McKendrick AM. The open perimetry interface: an enabling tool for clinical visual psychophysics. *J Vision*. 2012;12:22.
22. Dive S, Rouland JF, Lenoble Q, Szaffarczyk S, et al. Impact of peripheral field loss on the execution of natural actions. *J Glaucoma*. 2016;25:e889–e896.
23. Sunness JS, Applegate CA, Haselwood D, Rubin GS. Fixation patterns and reading rates in eyes with central scotomas from advanced atrophic age-related macular degeneration and Stargardt disease. *Ophthalmology*. 1996;103:1458–1466.
24. Duret F, Issenhuth M, Safran AB. Combined use of several preferred retinal loci in patients with macular disorders when reading single words. *Vision Res*. 1999;39:873–879.
25. McKee SP, Taylor DG. The precision of binocular and monocular depth judgments in natural settings. *J Vision*. 2010;10:5.
26. Bradshaw MF, Elliott KM, Watt SJ, Hibbard PB, Davies IRL, Simpson PJ Binocular cues and the control of prehension. *Spat Vis*. 2004;17:95–110.
27. Verghese P, Tyson TL, Ghahghaei S, Fletcher DC. Depth perception and grasp in central field loss. *Invest Ophthalmol Vis Sci*. 2016;57:1476–1487.

Appendix 1: Summary Figures of the 12 × 12 Glaucomatous Archetypes Interactions

Pictorial Summaries of IVFs of the Glaucomatous Archetypes Interactions

The pictorial summaries of the 144 IVFs of the 12 glaucomatous archetype interactions for the three planes are presented in Figures A1, A2, and A3 with the 12 archetypes ordered by VF defect location from superior to inferior and nasal to temporal.

Number of Locations with IVF Defects

The number of impaired locations (the *black squares*) at the anterior plane (25 cm), fixation plane (60 cm), and the posterior plane (100 cm) are summarized in Figures A4, A5, and A6, respectively. Although there may seem to be more impaired locations on the fixation plane (Fig. A5) than on both the anterior plane (Fig. A4) and posterior plane (Fig. A6) for the majority of archetype interactions, a closer examination of Figures A1, A2, and A3 suggests otherwise. There are generally more impaired locations on the anterior plane than the fixation plane. The numbers of impaired locations on the anterior plane but not on the fixation plane for all archetype interactions are summarized in Figure A7. In contrast, all locations with VF defects on the posterior plane display impaired vision on the fixation plane.

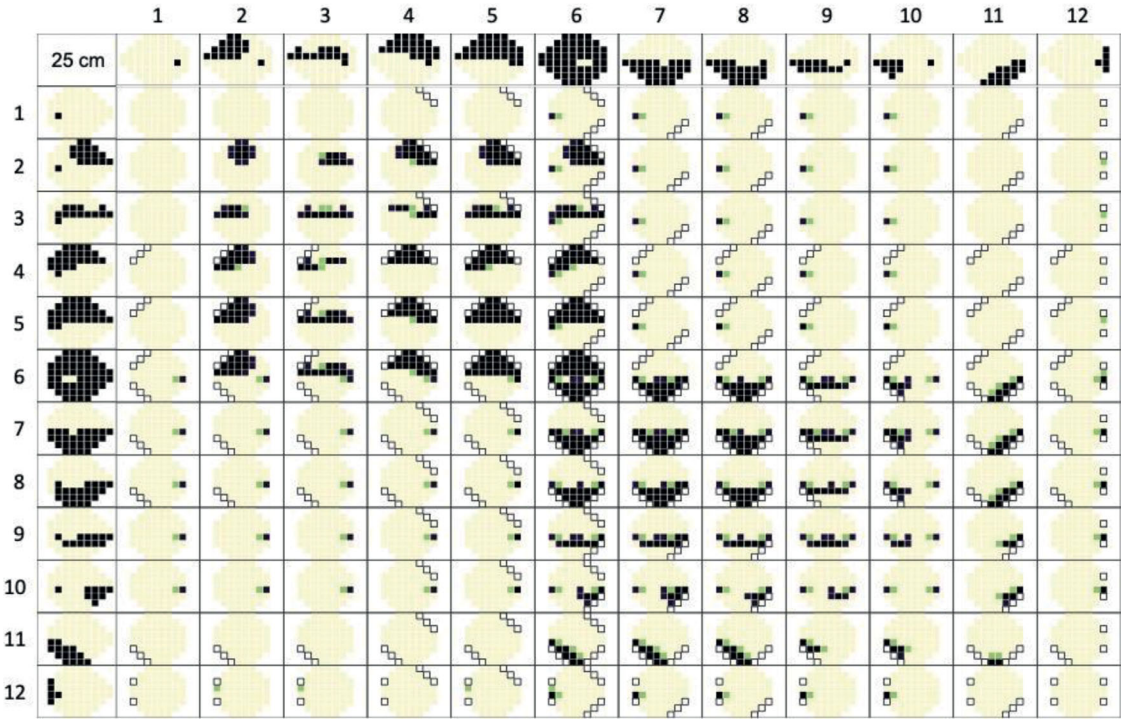

Figure A1. VF defect summary for the anterior plane for the 144 combinations of 12 archetypes with object distance at 25 cm and fixation at 60 cm. The archetypes are sorted by location of impairment (superior to inferior, nasal to temporal) and numbered 1 to 12 on the left side and the top. Locations in each subplot are color coded with darker value representing lower dB value; that is, *black*, 0 dB; *green*, 20 dB: and *yellow*, 30 dB. Any location with missing dB value is denoted by a *hollow square*.

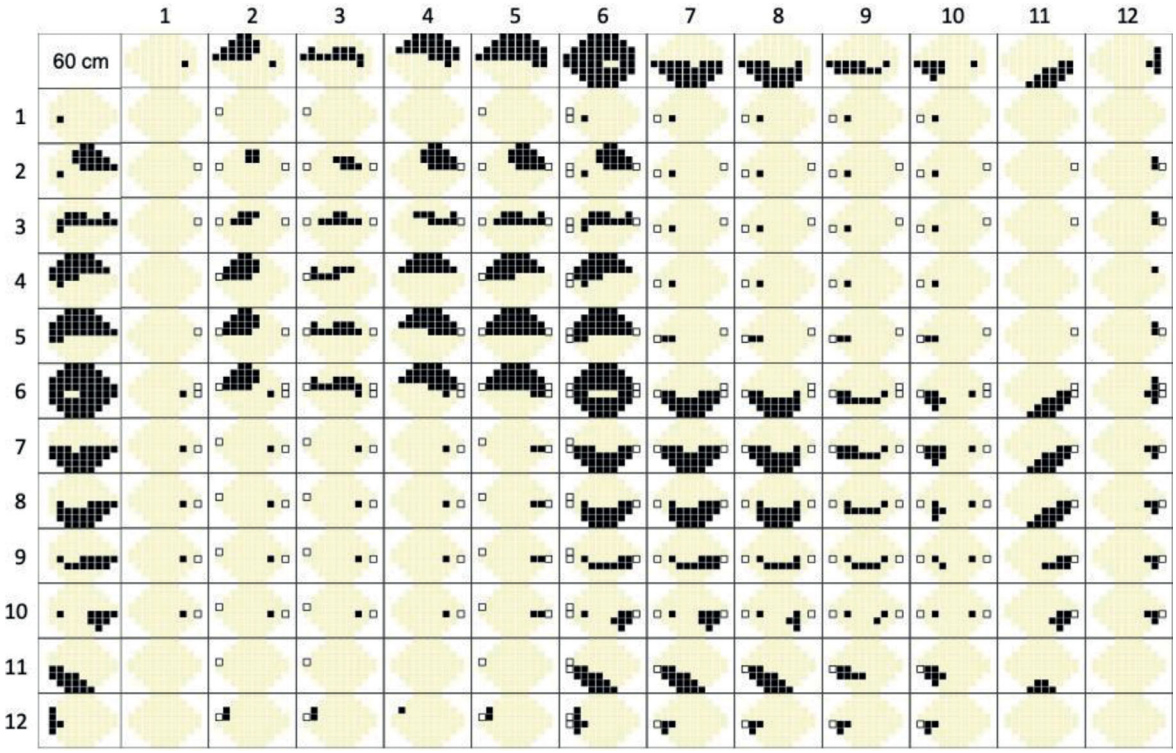

Figure A2. As in Figure A1, VF defect summary for the fixation plane with object distance at 60 cm and fixation at 60 cm.

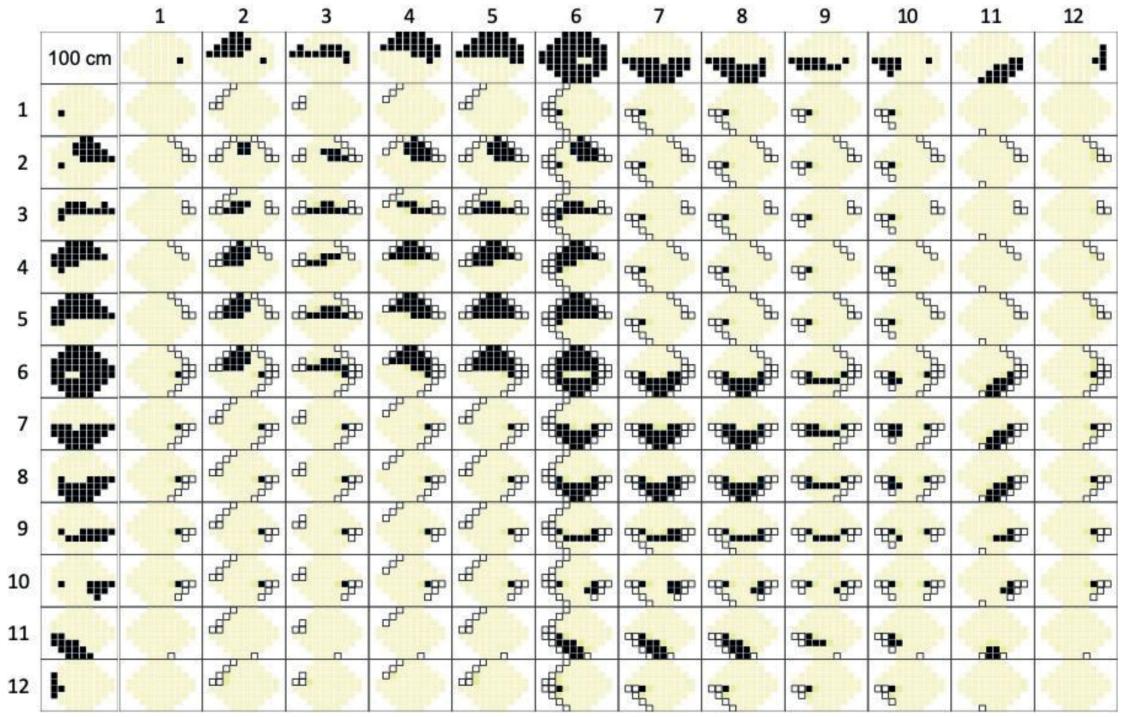

Figure A3. As in Figure A1, VF defect summary for the posterior plane with object distance at 100 cm and fixation at 60 cm.

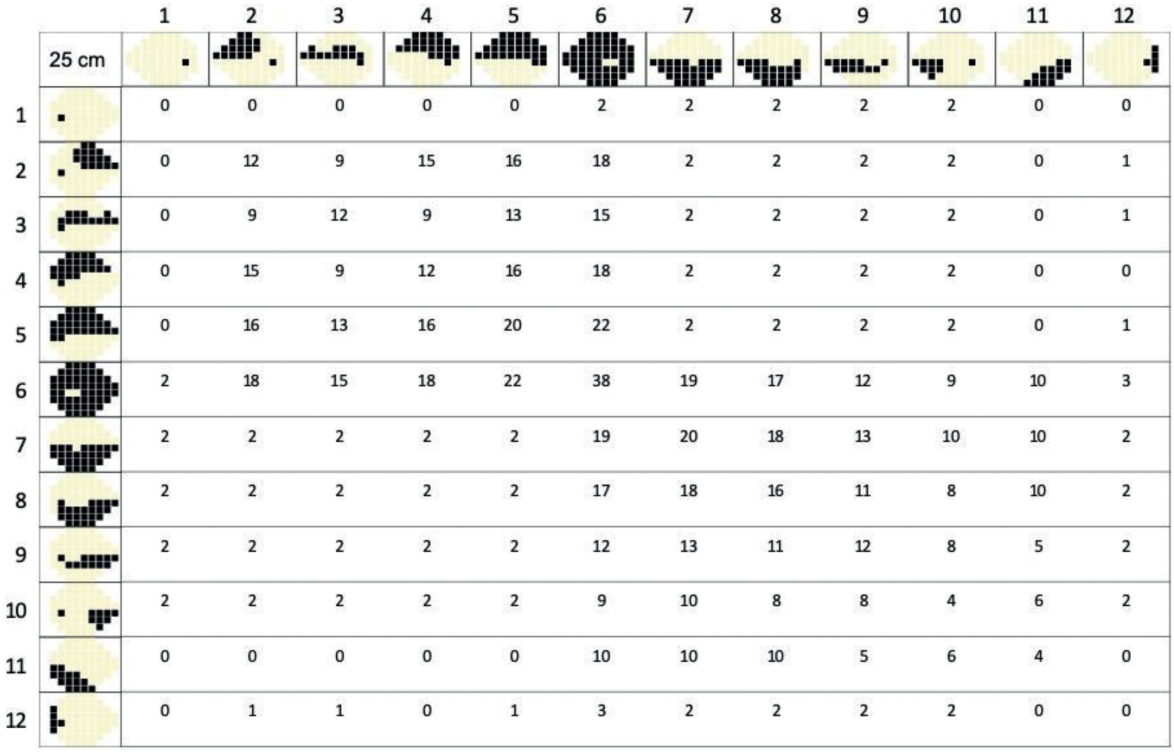

	1	2	3	4	5	6	7	8	9	10	11	12
1	0	0	0	0	0	2	2	2	2	2	0	0
2	0	12	9	15	16	18	2	2	2	2	0	1
3	0	9	12	9	13	15	2	2	2	2	0	1
4	0	15	9	12	16	18	2	2	2	2	0	0
5	0	16	13	16	20	22	2	2	2	2	0	1
6	2	18	15	18	22	38	19	17	12	9	10	3
7	2	2	2	2	2	19	20	18	13	10	10	2
8	2	2	2	2	2	17	18	16	11	8	10	2
9	2	2	2	2	2	12	13	11	12	8	5	2
10	2	2	2	2	2	9	10	8	8	4	6	2
11	0	0	0	0	0	10	10	10	5	6	4	0
12	0	1	1	0	1	3	2	2	2	2	0	0

Figure A4. Number of locations with impaired vision at object distance of 25 cm for the 144 combinations of 12 archetypes with a fixation distance of 60 cm.

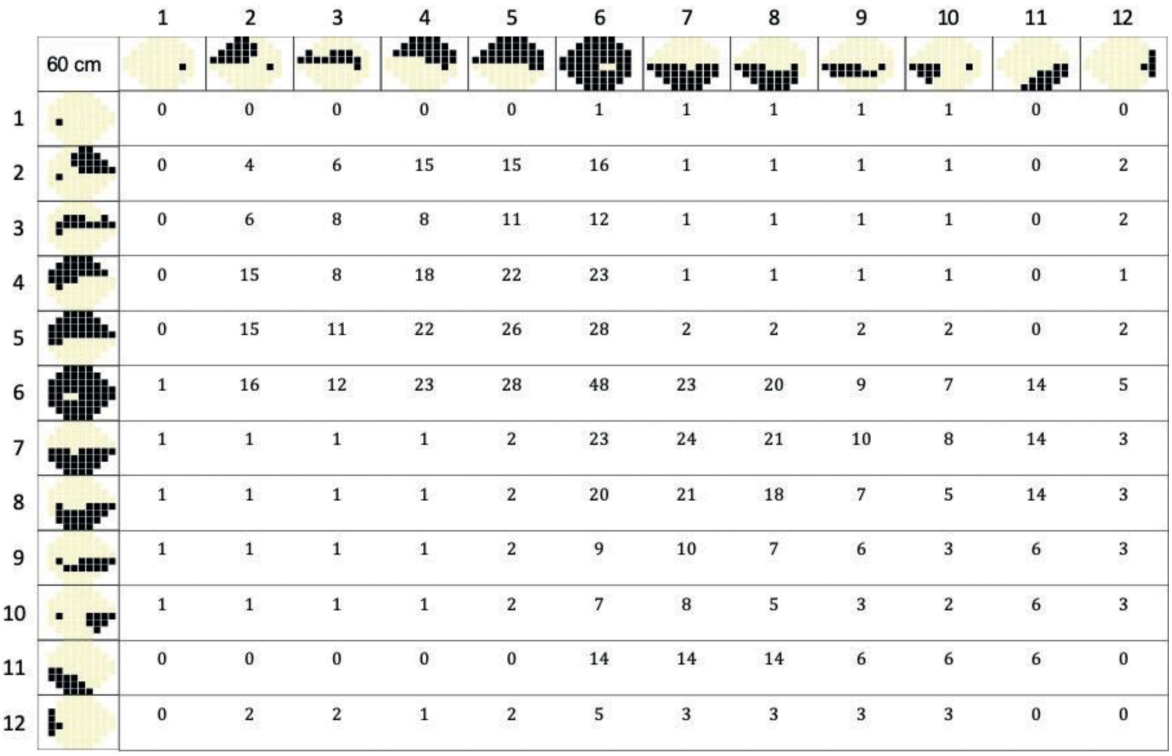

60 cm	1	2	3	4	5	6	7	8	9	10	11	12
1	0	0	0	0	0	1	1	1	1	1	0	0
2	0	4	6	15	15	16	1	1	1	1	0	2
3	0	6	8	8	11	12	1	1	1	1	0	2
4	0	15	8	18	22	23	1	1	1	1	0	1
5	0	15	11	22	26	28	2	2	2	2	0	2
6	1	16	12	23	28	48	23	20	9	7	14	5
7	1	1	1	1	2	23	24	21	10	8	14	3
8	1	1	1	1	2	20	21	18	7	5	14	3
9	1	1	1	1	2	9	10	7	6	3	6	3
10	1	1	1	1	2	7	8	5	3	2	6	3
11	0	0	0	0	0	14	14	14	6	6	6	0
12	0	2	2	1	2	5	3	3	3	3	0	0

Figure A5. Number of locations with impaired vision at object distance of 60 cm for the 144 combinations of 12 archetypes with a fixation distance of 60 cm.

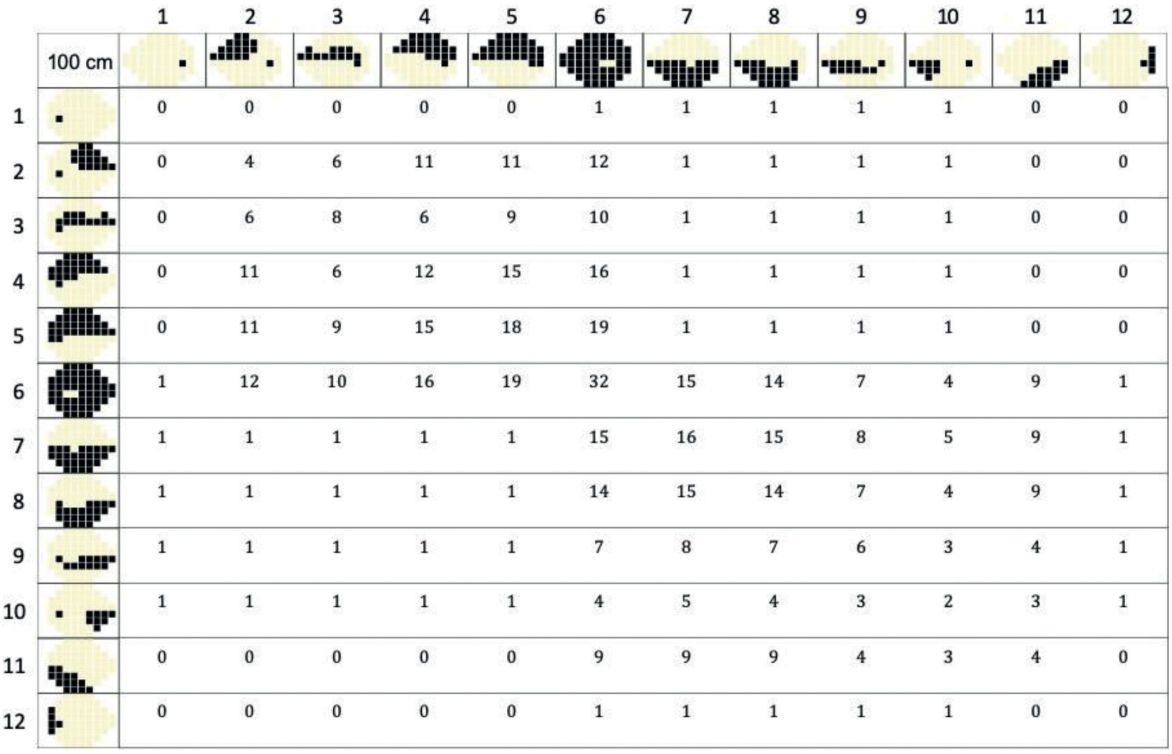

100 cm	1	2	3	4	5	6	7	8	9	10	11	12
1	0	0	0	0	0	1	1	1	1	1	0	0
2	0	4	6	11	11	12	1	1	1	1	0	0
3	0	6	8	6	9	10	1	1	1	1	0	0
4	0	11	6	12	15	16	1	1	1	1	0	0
5	0	11	9	15	18	19	1	1	1	1	0	0
6	1	12	10	16	19	32	15	14	7	4	9	1
7	1	1	1	1	1	15	16	15	8	5	9	1
8	1	1	1	1	1	14	15	14	7	4	9	1
9	1	1	1	1	1	7	8	7	6	3	4	1
10	1	1	1	1	1	4	5	4	3	2	3	1
11	0	0	0	0	0	9	9	9	4	3	4	0
12	0	0	0	0	0	1	1	1	1	1	0	0

Figure A6. Number of locations with impaired vision at object distance of 100 cm for the 144 combinations of 12 archetypes with a fixation distance of 60 cm.

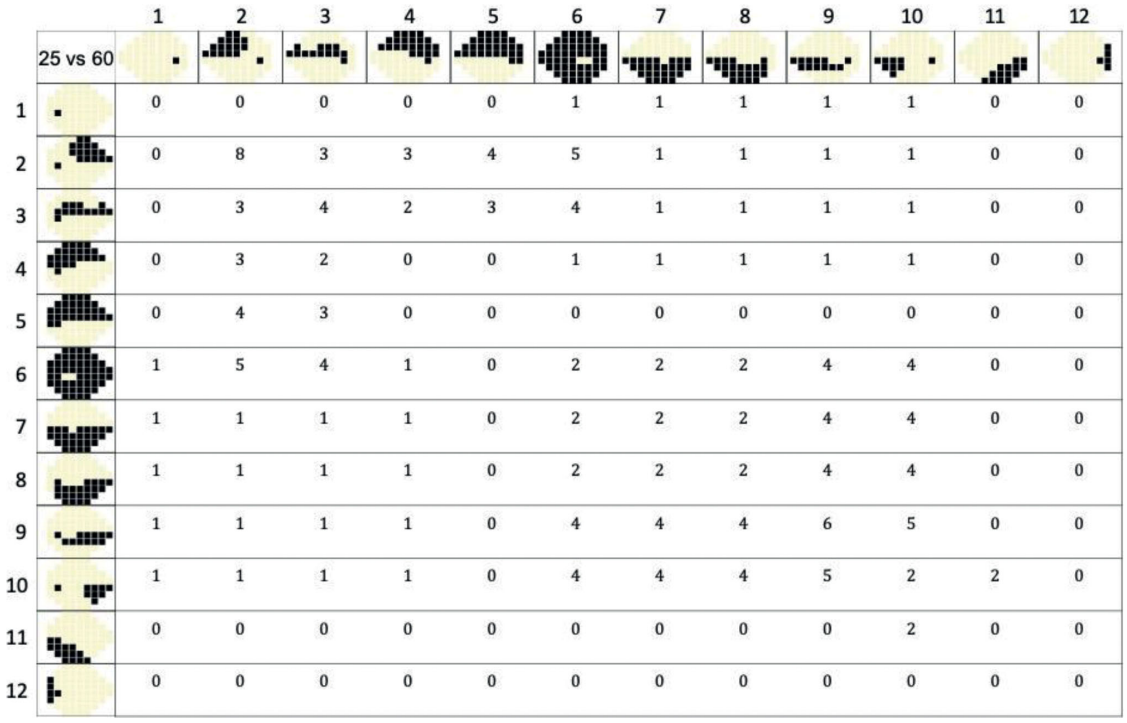

25 vs 60	1	2	3	4	5	6	7	8	9	10	11	12
1	0	0	0	0	0	1	1	1	1	1	0	0
2	0	8	3	3	4	5	1	1	1	1	0	0
3	0	3	4	2	3	4	1	1	1	1	0	0
4	0	3	2	0	0	1	1	1	1	1	0	0
5	0	4	3	0	0	0	0	0	0	0	0	0
6	1	5	4	1	0	2	2	2	4	4	0	0
7	1	1	1	1	0	2	2	2	4	4	0	0
8	1	1	1	1	0	2	2	2	4	4	0	0
9	1	1	1	1	0	4	4	4	6	5	0	0
10	1	1	1	1	0	4	4	4	5	2	2	0
11	0	0	0	0	0	0	0	0	0	2	0	0
12	0	0	0	0	0	0	0	0	0	0	0	0

Figure A7. Number of locations that are not impaired at fixation, but are impaired at object distance of 25 cm with a fixation distance of 60 cm for the 144 combinations of 12 archetypes.

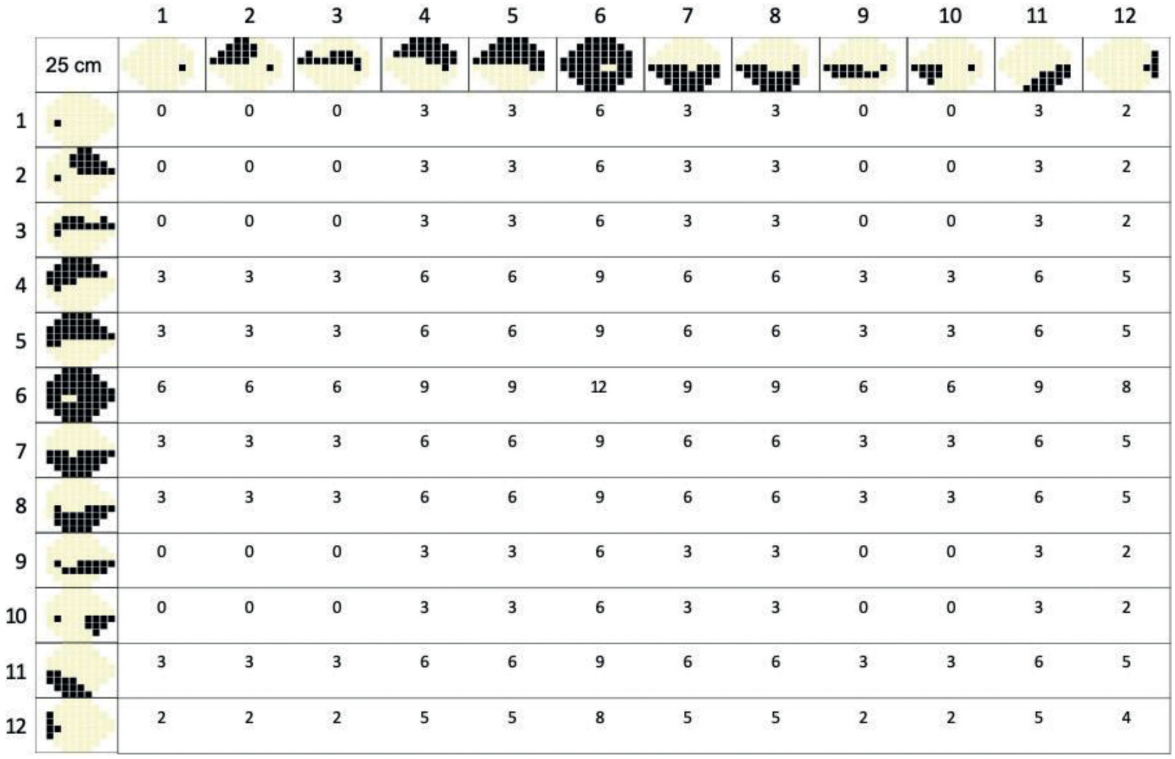

25 cm	1	2	3	4	5	6	7	8	9	10	11	12
1	0	0	0	3	3	6	3	3	0	0	3	2
2	0	0	0	3	3	6	3	3	0	0	3	2
3	0	0	0	3	3	6	3	3	0	0	3	2
4	3	3	3	6	6	9	6	6	3	3	6	5
5	3	3	3	6	6	9	6	6	3	3	6	5
6	6	6	6	9	9	12	9	9	6	6	9	8
7	3	3	3	6	6	9	6	6	3	3	6	5
8	3	3	3	6	6	9	6	6	3	3	6	5
9	0	0	0	3	3	6	3	3	0	0	3	2
10	0	0	0	3	3	6	3	3	0	0	3	2
11	3	3	3	6	6	9	6	6	3	3	6	5
12	2	2	2	5	5	8	5	5	2	2	5	4

Figure A8. Number of missing locations at object distance of 25 cm with a fixation distance of 60 cm for the 144 combinations of 12 archetypes.

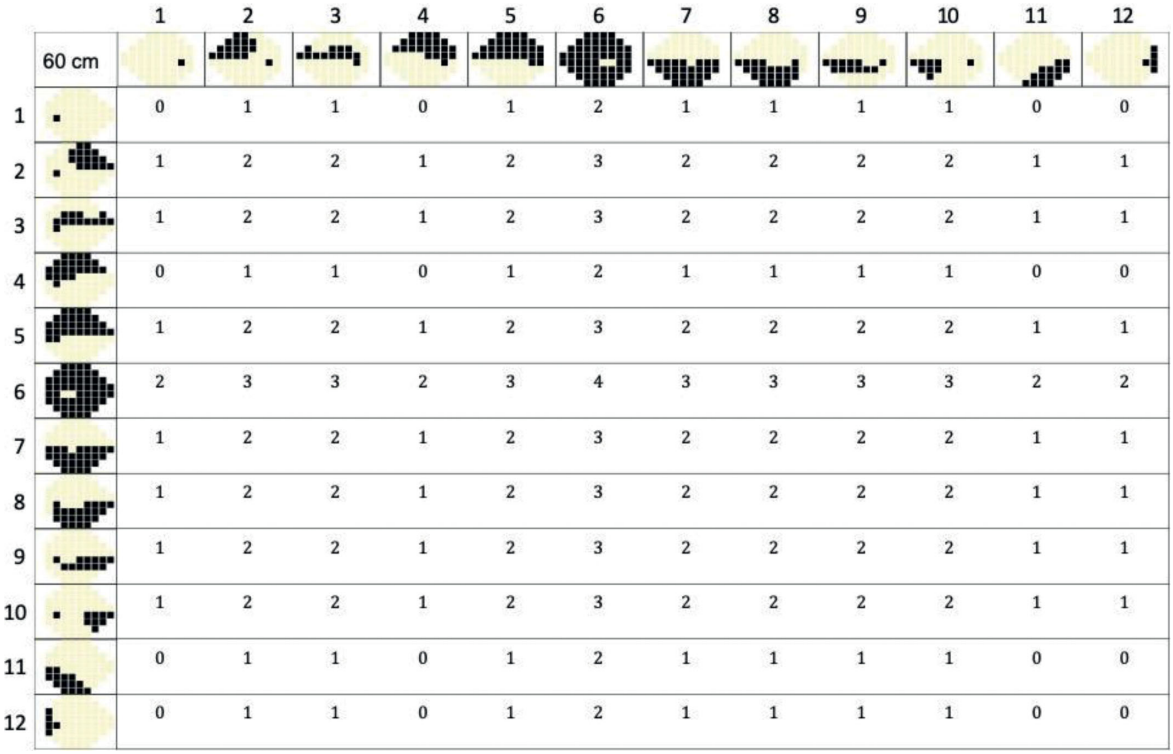

60 cm	1	2	3	4	5	6	7	8	9	10	11	12
1	0	1	1	0	1	2	1	1	1	1	0	0
2	1	2	2	1	2	3	2	2	2	2	1	1
3	1	2	2	1	2	3	2	2	2	2	1	1
4	0	1	1	0	1	2	1	1	1	1	0	0
5	1	2	2	1	2	3	2	2	2	2	1	1
6	2	3	3	2	3	4	3	3	3	3	2	2
7	1	2	2	1	2	3	2	2	2	2	1	1
8	1	2	2	1	2	3	2	2	2	2	1	1
9	1	2	2	1	2	3	2	2	2	2	1	1
10	1	2	2	1	2	3	2	2	2	2	1	1
11	0	1	1	0	1	2	1	1	1	1	0	0
12	0	1	1	0	1	2	1	1	1	1	0	0

Figure A9. Number of missing locations at object distance of 60 cm with a fixation distance of 60 cm for the 144 combinations of 12 archetypes.

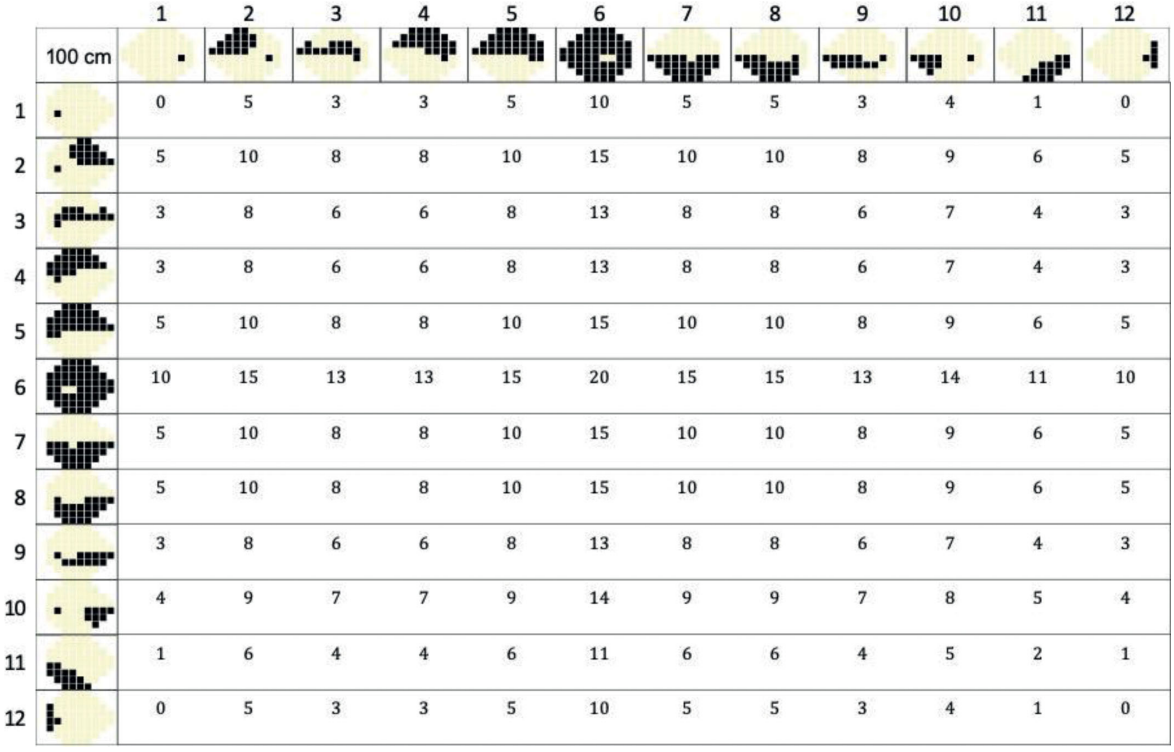

100 cm	1	2	3	4	5	6	7	8	9	10	11	12
1	0	5	3	3	5	10	5	5	3	4	1	0
2	5	10	8	8	10	15	10	10	8	9	6	5
3	3	8	6	6	8	13	8	8	6	7	4	3
4	3	8	6	6	8	13	8	8	6	7	4	3
5	5	10	8	8	10	15	10	10	8	9	6	5
6	10	15	13	13	15	20	15	15	13	14	11	10
7	5	10	8	8	10	15	10	10	8	9	6	5
8	5	10	8	8	10	15	10	10	8	9	6	5
9	3	8	6	6	8	13	8	8	6	7	4	3
10	4	9	7	7	9	14	9	9	7	8	5	4
11	1	6	4	4	6	11	6	6	4	5	2	1
12	0	5	3	3	5	10	5	5	3	4	1	0

Figure A10. Number of missing locations at object distance of 100 cm with a fixation distance of 60 cm for the 144 combinations of 12 archetypes.

Number of Locations with Missing Values

The number of locations with missing values for all archetype interactions are summarized in Figures A8, A9, and A10 for respective planes.

Appendix 2: Examples of Using the DD-IVF Functions

There are four main functions for DD-IVF simulation (makevf, caltheta, binovfcal) and visualization (plotvf). Additionally, the function rundemo runs the two Shiny apps included in the package. The following example briefly explains the usage of these functions.

For simulating the DD-IVFs, the monocular visual field (VF) data files should contain a minimum number of variables:

- ID: patient ID
- Eye: left (OS) or right (OD) eye
- VF data: 24-2 VF data (54 data points). The 54 data points must be ordered from superior nasal to inferior temporal.

In addition, there are two optional variables:

- pd: interpupillary distance (mm)
- Gender: patient gender used to estimate interpupillary distance when it is not available.

Load a VF csv File

To load a csv data file in to a data frame, the generic function `read.csv(filename)`

```
bino.df <- read.csv("/Users/david/vf/data/binocular.csv")
ID      <- bino.df$ID
Gender  <- bino.df$Gender
```

Create VF Matrices

The VF data for left and right eyes can be extracted from the loaded `bino.df` data frame.

```
left_visual_fields <- bino.df[bino.df$Eye=="OS", 4:ncol(bino.df)]
rght_visual_fields <- bino.df[bino.df$Eye=="OD", 4:ncol(bino.df)]
```

To convert the VF vectors to matrices for all patients, one can initialize a VF array for each eye for all patients then call the function `makevf` to store all data in the left and right VF arrays.

```
#initialize a vf array for all patients
vf_matrix     <- matrix(NA, ncol=10, nrow = 8)
left_vf_array <- replicate(nrow(left_visual_fields), vf_matrix)
rght_vf_array <- replicate(nrow(rght_visual_fields), vf_matrix)

#convert the vector data to matrices for the left and right eye
for (i in 1:nrow(left_visual_fields)){
  left_vf_array[,,i] <- makevf(unlist(left_visual_fields[i,],
                                use.names = F), eye="left")
}
for (i in 1:nrow(rght_visual_fields)){
  rght_vf_array[,,i] <- makevf(unlist(rght_visual_fields[i,],
                                use.names = F), eye="right")
}
```

Extract Individual Patient Data

VF matrices and gender information can be extracted from respective data structure by patient's ID.

```
id      <- 3
pindex  <- match(id, ID)
left_vf <- left_vf_array[, , pindex]
rght_vf <- rght_vf_array[, , pindex]
gender  <- Gender[pindex]
```

Calculate the Angle of Convergence

The angle of convergence is calculated using function `caltheta`. To calculate this angle, interpupillary distance and fixation distance values are required. The Cartesian coordinates of a fixation point are defined by a two-element vector. When the interpupillary distance is unavailable, one can provide gender information (female or male) and respective population mean value will be used.

```
fix_dist   <- c(600, 0)
theta_left <- caltheta(fix_dist, gender = gender, eye = "left")
theta_rght <- caltheta(fix_dist, gender = gender, eye = "right")
```

Calculate IVF for All Distance Planes

The function `binovfcal` returns the simulated IVF data in an array for all specified object distances. It requires 6 arguments: left and right VF matrices, left and right convergence angles, a vector specifying object distance planes and interpupillary distance or gender.

```
object_distances <- seq(300, 1000, 50)
ivfs             <- binovfcal(left_vf, rght_vf,
                              theta_left, theta_rght,
                              object_distances,
                              gender=gender)
```

Subsetting

Each matrix in the output array of the function `binovfcal` is named by corresponding object

distance value. For example, to extract the IVF for the object distance at 500 mm, one way is as the following

```
ivf <- ivfs[, , as.character(500)]
```

Visualization

The function `plotvf` plots both monocular VFs or simulated IVFs. The following code returns all plots for each distance plane specified in the `object_distances` vector into a pdf file. The function `colorkey` plots the color-coding scheme used by the function `plotvf`.

```
filename <- paste0("DD-IVF", id, ".pdf")
pdf(filename, width=16)
options(error=dev.off)
layout(matrix(c(1, 1, 1, 1, 1, 1, 2, 4, 5, 3, 4, 5), 3, 4),
       heights = c(3, 3, 1))

for (i in object_distances) {
  plotvf(m_xs, left_vf, "Left Monocular")
  plotvf(m_xs, rght_vf, "Right Monocular")
  plotvf(c_xs, ivfs[, , as.character(i)],
               paste0("Fixation Distance = ", fix_dist[1],
                      "mm, Object Distance = ", i, "mm"))
  colorkey()
}

dev.off()
options(error=NULL)
```